Polymer Degradation and Stability 232 (2025) 111147

Contents lists available at ScienceDirect

Polymer Degradation and Stability

journal homepage: www.journals.elsevier.com/polymer-degradation-and-stability

# In-situ co-precipitation synthesis of Zn/Fe-LDH modified melamine polyphosphate for enhanced flame retardancy in polypropylene

Zhishuo Liu [a,b,1], Yifang Hua [b,1], Suqin Liu [a], Hongfei Li [b], Xiaoyu Gu [b], Jun Sun [b,*], Sheng Zhang [b,*]

[a] Shandong Institute of Non-metallic Materials, Jinan, China
[b] State Key Laboratory of Organic-Inorganic Composites, Beijing University of Chemical Technology, Beijing, China

ARTICLE INFO

*Keywords:*
Polypropylene
Intumescent flame retardant
Layered double hydroxide

ABSTRACT

In this study, a novel approach was employed to enhance the flame retardant efficiency of an intumescent flame retardant (IFR) by growing a layered double hydroxides (LDHs) of Zn/Fe on the surface of melamine polyphosphate (MPP), denoted as Zn/Fe-LDH@MPP (LDHMPP). This modification was carried out via in-situ co-precipitation, and the resulting composite was subsequently applied to polypropylene (PP) in conjunction with piperazine pyrophosphate (PAPP). Under the same proportion and concentration, the PP/16 %LDHIFR formulation achieved a preferred V-0 rating in the UL-94 test. Furthermore, this formulation exhibited an enhanced ability to form a protective char layer, as evidenced by both cone calorimetry tests (CCT) and thermogravimetric analysis (TGA) tests. Additionally, the synergistic effect of Zn/Fe-LDH on flame retardancy was also studied.

## 1. Introduction

Polypropylene (PP), a ubiquitous thermoplastic resin, has found extensive utilization across various industrial sectors [1–3], including automotive, chemical, and construction, owing to its remarkable attributes, such as exceptional corrosion resistance and favorable mechanical properties [4–6]. Nonetheless, it exhibits a significant drawback in terms of its high flammability without the inherent ability to form a protective char layer [7–9]. In the event of ignition, PP undergoes rapid heat release and produces copious molten droplets, thereby imposing substantial limitations on its applicability across diverse industrial domains [10]. Hence, there is a critical need to enhance the flame retardancy of PP [11].

Presently, prevalent flame-retardant additives employed in PP encompass brominated compounds, inorganic agents, phosphorus/nitrogen-based flame retardants, and intumescent flame retardants (IFR) [12–14]. Among these options, IFR comprise components including acids, gas-forming agents, and carbon sources [15]. In contrast to halogen-based flame retardants, IFR exhibits reduced environmental impact [16]. Among these alternatives, the melamine polyphosphate/piperazine pyrophosphate (MPP/PAPP) system emerges as one of the most typical IFR formulation [17–19]. Nevertheless, conventional IFR systems exhibit certain drawbacks, notably suboptimal flame-retardant efficiency [20], necessitating substantial additions to achieve desirable flame-retardant characteristics, thereby adversely affecting the mechanical properties [21]. Therefore, how to economically improve the negative effects of IFR on the mechanical properties of PP, while improving the flame retardant efficiency, is an important research topic [22–24].

Layered double hydroxides (LDHs) have been widely used in flame retardant research, presenting a pronounced layered structure with interlayer ions and water molecules arranged in such a way as to involve them overlapping with each other [25]. Its distinctive structural features demonstrate a remarkable synergistic capability within flame retardant systems, while the inherent moisture content in LDH contributes to the reduction of polymer ignition temperatures during combustion [26]. Nevertheless, the use of LDH as a standalone flame retardant necessitates a higher loading concentration to achieve efficacy, resulting in a more pronounced influence on the mechanical characteristics of the polymer [27].

Taking into account the above effects, the strategy of using LDHs to modify flame retardants is a feasible way to improve flame-retardant efficiency [28]. Hu et al [29] developed core-shell structured flame retardant composite materials (CMSs@LDHs) for improving flame

* Corresponding authors.
*E-mail addresses:* sunj@mail.buct.edu.cn (J. Sun), zhangsheng@mail.buct.edu.cn (S. Zhang).
[1] The authors contributed equally to this work.

https://doi.org/10.1016/j.polymdegradstab.2024.111147
Received 6 September 2024; Received in revised form 11 December 2024; Accepted 12 December 2024
Available online 13 December 2024

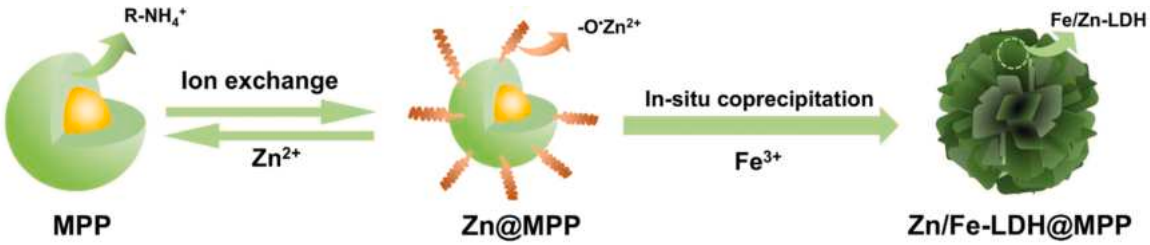


**Fig. 1.** Roadmap for the synthesis of Zn/Fe-LDH@MPP.

retardant efficiency. This approach involved the growth of LDHs on the surface of carbon microspheres (CMSs). CMSs@LDHs exhibited excellent flame retardancy, achieving a V-0 rating and significantly elevating the LOI to 28.9 % when incorporated at a loading of 20 wt% in PP matrix. To address the uniform dispersion of LDHs within matrix, Wang et al [30] used LDHs as the nucleus and tannic acid and phosphonitrile crosslinked polymer network (TA-HP) as the shell, to obtain the nucleus-shell structure named as LDH@TA-HP. When incorporated at a concentration of 20 wt% LDH@TA-HP in the PP, it achieved a V-0 rating. This approach also magnified the "zig-zag path" effect of LDHs, contributing to its improved performance as a flame retardant. However, the above methods still lacked sufficient efficiency and incurred high production costs, making it challenging to promote industrial applications.

In this study, a novel flame retardant, Zn/Fe-LDH@MPP (LDHMPP), was synthesized through an in-situ co-precipitation method, and incorporated with PEPA to form IFR, achieving higher flame retardant effect than MPP/PEPA. Interestingly, LDHMPP had a positive effect on mechanical properties. This investigation was anticipated to offer a solution for achieving the desired balance between flame retardancy and mechanical properties in PP composites.

## 2. Experimental

### 2.1. Materials

Polypropylene (PP, MFI: 2.6 g/10 min) was procured from Maoming Petrochemical Co., Ltd., China, while melamine polyphosphate (MPP) was obtained from Zhenjiang Star Flame Retardant Co., Ltd. The piperazine pyrophosphate (PAPP, with a whiteness exceeding 95 %) was sourced from Chongqing Kejufu New Material Co. Ltd. Zinc nitrate hexahydrate ($Zn(NO_3)_2{\cdot}6H_2O$, >99.0 %) and ferric nitrate nonahydrate ($Fe(NO_3)_3{\cdot}9H_2O$, ≥98.5 %) were purchased from Shanghai Aladdin Chemical Reagents Co., China. The ethanol and aqueous ammonia were acquired from Sinopharm Chemical Reagent Co., Ltd. (Nanjing, Jiangsu, China). All chemicals employed in this study were analytical grade and used without further purification.

### 2.2. Synthesis of Zn/Fe-LDH

4.5 g $Zn(NO_3)_2{\cdot}6H_2O$ and 3.0 g $Fe(NO_3)_3{\cdot}9H_2O$ were fully dissolved in 200 mL of ethanol and stirred 0.5 h Following this, aqueous ammonia was added to the above solution to adjust the pH to the range of 9.5–10. Then the solution temperature was elevated to 50 °C, and was sustained for 12 h to accomplish co-precipitation. After filtration, the solid product was washed with water until neutral to remove nitrates, followed by five washes with ethanol, and subsequently dried in an oven at 80 °C for 12 h The abbreviation of Zn/Fe-LDH was LDH.

### 2.3. Synthesis of Zn/Fe-LDH@MPP

4.5 g $Zn(NO_3)_2{\cdot}6H_2O$ and 10 g MPP were completely dispersed in 200 mL ethanol and stirred at room temperature for 2 h Then, 3 g $Fe(NO_3)_3{\cdot}9H_2O$ was dissolved in 200 mL ethanol and added to the above solution, and the stirring was continued for 0.5 h Subsequently, aqueous ammonia was added dropwise to adjust the pH to 9.5–10, continued to stir for 2 h, and then reacted at 50 °C for 12 h Finally, the product was obtained by filtration, washed five times, and dried in an oven at 80 °C. The synthesis route of Zn/Fe-LDH@MPP (LDHMPP) was shown in Fig. 1.

**Table 1**
The formulations of PP composites.

| Sample | Formula | | | | |
|---|---|---|---|---|---|
| | PP (wt%) | PAPP (wt%) | MPP (wt%) | LDHMPP (wt%) | LDH (wt%) |
| PP | 100 | 0 | 0 | - | 0 |
| PP/16 %IFR | 84 | 11.2 | 4.8 | - | 0 |
| PP/14 %IFR/2 %LDH | 84 | 9.8 | 4.2 | - | 2.0 |
| PP/16 %LDHIFR | 84 | 11.2 | 0 | 4.8 | 0 |

### 2.4. Preparation of PP composites

The PP and additives were blended, followed by a melt-blending process in an internal mixer for 6 mins. The temperature in the three zones of the mixer was maintained at 180 °C, and the blending speed was set at 50 rpm. These materials were subsequently subjected to a hot pressing procedure at 15 MPa and 185 °C, for 15 mins using a flat-plate vulcanizer, resulting in the formation of 3.2 mm samples that were subsequently cut for conducting flame retardant tests.

For testing the mechanical properties, standard specimens were produced using a micro-injection molding machine under the conditions of 220 °C and 8 MPa. The complete formulation for the PP composite materials can be found in Table 1. The IFR ratio was set to PEPA/MPP (or LDHMPP) = 7/3.

### 2.5. Characterization methods

The in-situ co-precipitation of Zn/Fe-LDH@MPP was monitored using Fourier transform infrared spectroscopy (FTIR). The experiments were conducted with an iS-5 FTIR spectrometer (Nicolet Instrument, USA), employing 64 scans and a resolution of 4 $cm^{-1}$, within the spectral range of 4000 $cm^{-1}$ to 500 $cm^{-1}$. The samples were prepared by uniformly grinding and pressing the samples and KBr powder into tablets. The mass ratio of the samples to KBr powder was approximately 1:100.

The X-ray diffraction (XRD) patterns were acquired using a Rigaku D/MAX-2600 instrument from Japan, with a scanning range spanning 5° to 80° and a scanning speed of 5°/min.

The morphology, fracture appearances, and char residue of the Zn/Fe-LDH@MPP composites were examined using scanning electron microscopy (SEM) with an S-4700 instrument (Hitachi, Japan) operating at 20 kV acceleration voltage. The elemental composition was analyzed using energy dispersive X-ray spectroscopy (EDS). Prior to detection, all samples were coated with Pt.

Thermogravimetric analysis (TGA) was conducted using a Q50 apparatus from TA Instruments. All samples were heated at a rate of 10 °C/min from room temperature to 800 °C in flowing $N_2$. The sample mass ranged from 3 to 5 mg.

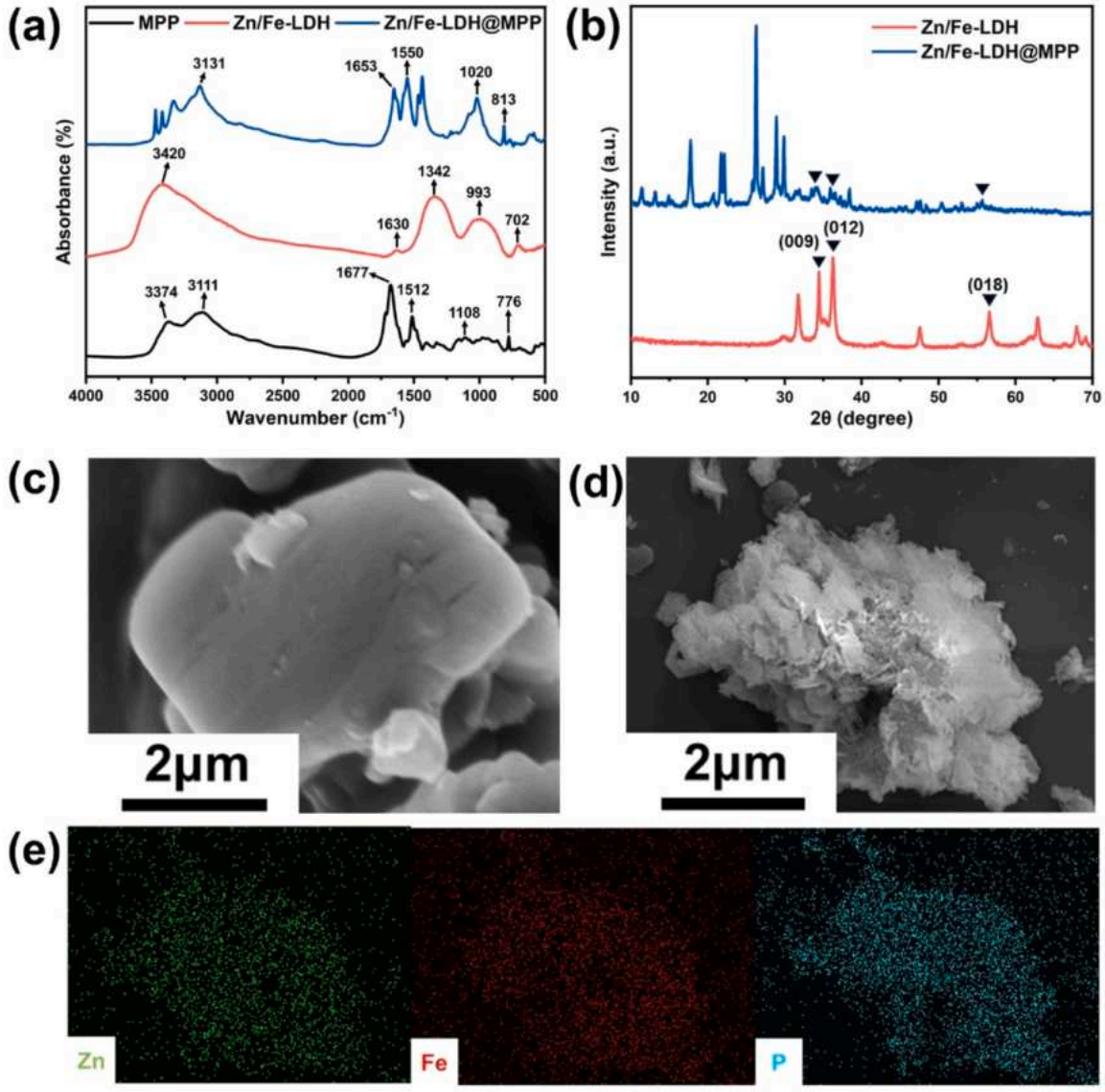


**Fig. 2.** (a) FTIR spectra, (b) XRD, SEM image of (c) MPP and (d) Zn/Fe-LDH@MPP, and (e) EDS mapping of Zn/Fe-LDH@MPP.

The limiting oxygen index (LOI) was determined using a Model JF-3 oxygen index instrument (Nanjing Jiangning District Instrument Manufacturing Factory, China) with sheet dimensions of 130 mm × 6.5 mm × 3 mm, following ISO 4589-1996. The UL-94 vertical burning test (UL-94) was carried out using a JF-3 type horizontal and vertical burning tester (Jiangning Analysis Instrument Company, China) with specimen dimensions of 130 mm × 13 mm × 3.2 mm, following ISO 9773.

The cone calorimeter test was conducted using a cone calorimeter machine (Fire Test Technology Co. Ltd, UK) in accordance with the ISO-5660 standard at a heat flux of 50 kW/m$^2$. Each specimen, sized at 100 mm × 100 mm × 3 mm, was tested.

The mechanical properties tests were performed using an XJJ-5 instrument (Jinjian Testing Instrument Co., Ltd., China) following ISO 527–1 standard. The samples were tested at a speed of 10 mm/min.

## 3. Results and discussion

### 3.1. Characterization of Zn/Fe-LDH@MPP

The FTIR spectra was presented in Fig. 2, in the case of Zn/Fe-LDH, the appearance of peaks at 3420 cm$^{-1}$ and 1630 cm$^{-1}$ [31] indicated the involvement of -OH stretching and bending vibrations associated with interlayer and interlayer water molecules. The peak at 1342 cm$^{-1}$ corresponded to the antisymmetric stretching of interlayer carbonate species [32]. Furthermore, the vibrational peaks at 993 cm$^{-1}$ and 702 cm$^{-1}$ [33] were indicative of the presence of $Fe^{3+}$ and $Zn^{2+}$ ions within the LDH structure.

Upon the in-situ co-precipitation of Zn/Fe-LDH on the surface of MPP, noteworthy changes were observed in the FTIR spectrum. The broad -OH vibration peak at 3374 cm$^{-1}$ from MPP diminished, signifying a reduction in surface hydroxyl groups. The -$NH^{3+}$ peak underwent a shift to 3131 cm$^{-1}$ [34], suggesting altered chemical interactions. Moreover, the vibrational modes associated with the triazine ring, C═N bonds, P═O, and P—O—P bonds exhibited shifts and alterations in peak shape [35,36], with notable peaks at 1653 cm$^{-1}$, 1550 cm$^{-1}$, 1020 cm$^{-1}$, and 813 cm$^{-1}$, respectively.

The chemical composition of Zn/Fe-LDH@MPP was characterized by XRD showed in Fig. 2(b). Peaks at 2θ values of 34.5°, 36.3°, and 56.6° were observed in Zn/Fe-LDH [37–40], corresponding to the (009), (012), and (018) planes, respectively. The corresponding characteristic peaks were also present in the curve of Zn/Fe-LDH@MPP. The surface

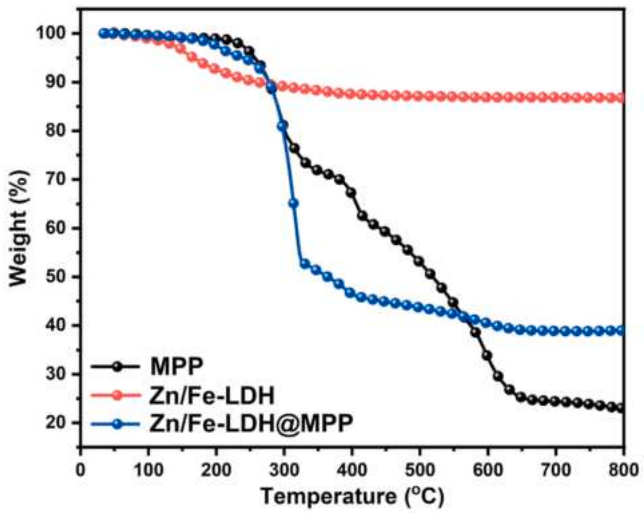


**Fig. 3.** The TGA curves of MPP, Zn/Fe-LDH and Zn/Fe-LDH@MPP.

**Table 2**
Some related data of MPP, Zn/Fe-LDH and Zn/Fe-LDH@MPP in TGA test.

| Sample | $T_{5\ \%}$ (°C) | $T_{max}$ (°C) | Residue char (%) |
|---|---|---|---|
| MPP | 257 | 295 | 23.3 |
| Zn/Fe-LDH | 240 | 314 | 86.9 |
| Zn/Fe-LDH@MPP | 162 | 149 | 39.3 |

characteristics and elemental composition of Zn/Fe-LDH@MPP were analyzed and the results are shown in Fig. 2 (c) and (d). MPP exhibited a smooth particle surface in the SEM images. In stark contrast, the surface morphology of Zn/Fe-LDH@MPP displayed pronounced roughness and the presence of nanoparticles, which was clearly characterized by an orderly and uniform layered structure. Furthermore, EDS analysis confirmed the even distribution of Fe and Zn elements across the surface of Zn/Fe-LDH@MPP. Specifically, the P content in Zn/Fe-LDH@MPP had decreased from 2.35 wt% (in MPP) to 0.59 wt%, while the content of Fe and Zn elements had increased to 3.21 wt% and 4.29 wt%, respectively. These modifications were indicative of the successful loading of Zn/Fe-LDH onto the surface of MPP.

### 3.2. Thermal stability

The thermogravimetric analysis (TGA) curves of MPP, Zn/Fe-LDH, and Zn/Fe-LDH@MPP under a $N_2$ atmosphere were depicted in Fig. 3, and Table 2. MPP underwent a three-stage degradation process. The first stage, occurring around 290 °C, can be attributed to the decomposition of MPP, resulting in the release of $NH_3$ and $H_2O$ gases and the formation of a polyphosphoric acid layer. The second stage, around 400 °C, involved further decomposition leading to the formation of phosphates. The third stage, at approximately 600 °C, decomposed to establish a more stable char layer structure.

The decomposition mode of Zn/Fe-LDH@MPP was similar to that of MPP, but the maximum weight loss rate ($R_{max}$) in the first stage was significantly higher. This heightened rate was attributed to the earlier thermal decomposition of Zn/Fe-LDH, which in turn promoted the earlier action of the flame retardant. At the same time, Zn/Fe-LDH exhibited greater resistance to further decomposition, resulting in a significantly elevated char residue (39.3 %) at 800 °C compared to MPP.

The thermogravimetric analysis of PP composites was shown in Fig. 4 and Table 3. Pure PP exhibited limited char-forming ability, undergoing single-step degradation with only 0.4 wt% char residue at 700 °C. The addition of 16 wt% IFR improved the char-forming ability, increasing the final char residue to 7.3 wt%. However, IFR decomposition led to an earlier onset of thermal degradation, reducing the $T_{5\ \%}$ to 396 °C. The introduction of the synergistic agent Zn/Fe-LDH further enhanced the char-forming performance. This improvement was reflected in the reduction of $R_{max}$ from 3.1 %/°C in the control sample to 1.3 %/°C. Notably, PP/16 %LDHIFR exhibited superior thermal decomposition suppression, with an $R_{max}$ of only 1.1 %/°C and a significant increase in char residue to 10.2 wt%. These results demonstrate

**Table 3**
TGA and DTG data of PP and its composites.

| Sample | $T_{5\ \%}$ (°C) | $R_{max}$ (%/°C) | Char yield at 700 °C (wt%) |
|---|---|---|---|
| PP | 436 | 3.1 | 0.4 |
| PP/16 %IFR | 396 | 2.9 | 7.3 |
| PP/14 %IFR/2 %LDH | 358 | 1.3 | 8.9 |
| PP/16 %LDHIFR | 352 | 1.1 | 10.2 |

**Table 4**
The LOI and UL-94 rating of PP composites.

| Samples | LOI (%) | UL-94 | | |
|---|---|---|---|---|
| | | $t_1/t_2$(s) | Dripping | Rating |
| PP | 18.5 ± 0.2 | 52.0/- | Y | NR |
| PP/16 %IFR | 30.2 ± 0.2 | 45.0/- | Y | NR |
| PP/14 %IFR/2 %LDH | 31.3 ± 0.2 | 2.2/11.4 | N | V-1 |
| PP/16 %LDHIFR | 32.7 ± 0.2 | 1.1/3.3 | N | V-0 |

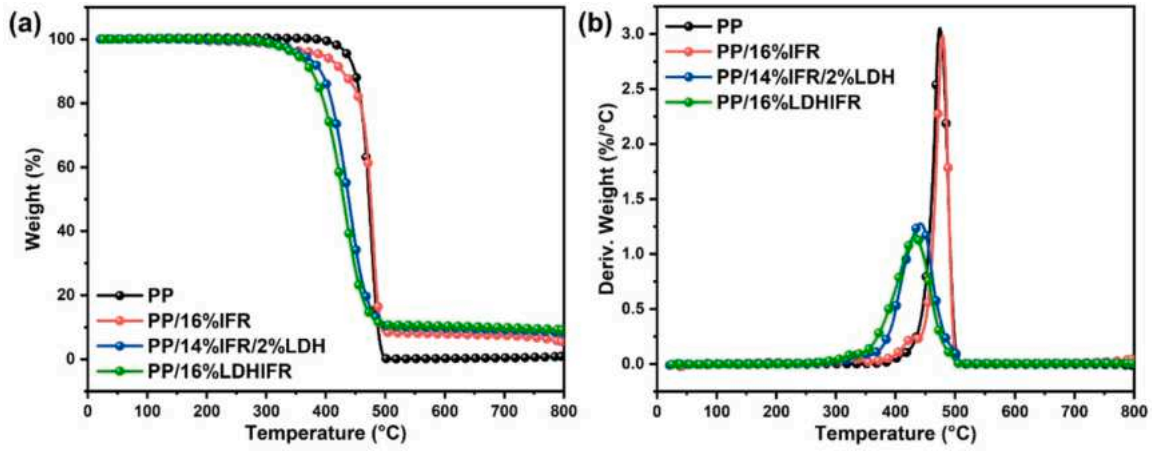


**Fig. 4.** TGA (a) and DTG (b) curves of PP, PP/16 %IFR, PP/14 %IFR/2 %LDH and PP/16 %LDHIFR under $N_2$ atmosphere.

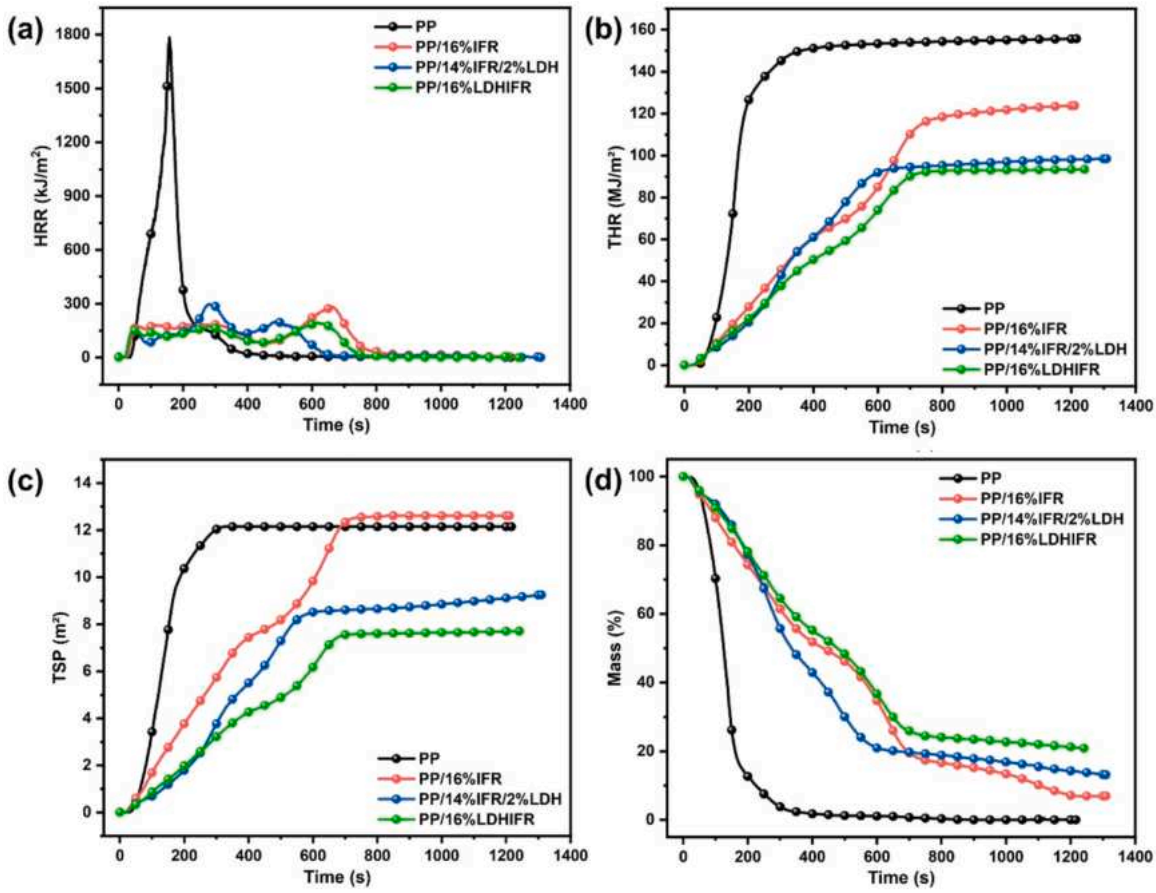


**Fig. 5.** PHRR (a), THR (b), TSP(c) and Mass (d) curves for different PP samples.

**Table 5**
PHRR, THR, TSP and specimen mass statistics of samples in cone test.

| Sample | pHRR ($kW/m^2$) | THR ($MJ/m^2$) | TSP ($m^2$) | Mass (%) |
|---|---|---|---|---|
| PP | 1789 ± 55 | 157 ± 7 | 12.2 ± 0.3 | 0.7 ± 0.1 |
| PP/16 %IFR | 298 ± 26 | 124 ± 5 | 13.1 ± 0.4 | 7.1 ± 0.2 |
| PP/14 %IFR/2 %LDH | 292 ± 24 | 98 ± 5 | 9.2 ± 0.2 | 13.8 ± 0.3 |
| PP/16 %LDHIFR | 185 ± 15 | 92 ± 6 | 7.6 ± 0.2 | 21.4 ± 0.1 |

that Zn/Fe-LDH@MPP exhibited a strong catalytic carbonization capability in the PP system.

### 3.3. Flame retardancy

To assess the flame retardancy of the PP composite materials, the results of LOI and UL-94 tests were summarized in Table 4. Pure PP exhibited a low LOI of only 18.5 %, and it received no UL-94 rating. Although upon the introduction of 16 wt% IFR into PP (PP/16 %IFR), the UL-94 test still did not get a rating, indicating that the flame retardancy remained inadequate. The composite was further refined by adding 2 wt% Zn/Fe-LDH as a flame retardant synergist. This led to a notable enhancement in flame retardant performance, resulting in a heightened LOI of 31.3 % and attaining a V-1 rating.

The subsequent introduction of PAPP and Zn/Fe-LDH@MPP to construct the IFR composite (PP/16 %LDHIFR). This composite exhibited a significantly elevated LOI of 32.7 % and achieved a V-0 rating in the UL-94 test. It was observed that PP/16 %LDHIFR demonstrated a more rapid formation of char and stronger self-extinguishing properties. This indicated that Zn/Fe-LDH@MPP possessed exceptional catalytic char-forming capabilities within the PP matrix.

To further confirm the outstanding flame retardancy of Zn/Fe-LDH@MPP in PP, cone calorimeter tests were employed. The curves depicting the heat release rate (HRR), total heat release (THR), total smoke production (TSP), and specimen mass were prominently displayed in Fig. 5 and Table 5. The pure PP sample ignited vigorously, characterized by a peak heat release rate (pHRR) of 1789 $kW/m^2$ and a THR of 157 $MJ/m^2$. However, upon the introduction of 16 wt% IFR into the PP matrix, the pHRR and THR decreased substantially to 298 $kW/m^2$ and 124 $MJ/m^2$, respectively. Nevertheless, the composite exhibited elevated smoke release, with a TSP of 13.1 $m^2$, indicative of gas-phase mechanisms. In the case of PP/14 %IFR/2 %LDH, the introduction of the synergist led to the formation of a higher-quality char layer within the flame-retardant system, significantly suppressing TSP to 9.2 $m^2$.

PP/16 %LDHIFR exhibited the lowest pHRR, THR and TSP, with only 185 $kW/m^2$,92 $MJ/m^2$ and 7.6 $m^2$, respectively. Additionally, the char residue content in PP/16 %LDHIFR was notably higher at 21.34 % compared to other samples, attributable to the uniform conjunction between Zn/Fe-LDH and MPP, resulting in the formation of a dense and expanded char layer during flame combustion.

### 3.4. Analysis of the char residue

In order to gain a deeper insight into the impact of IFR on the char residue formation in composite materials, the microstructure of the resulting char residues was analyzed using SEM. Fig. 6 illustrated the findings, revealing that pure PP underwent complete combustion with little char residue content. In stark contrast, the samples containing flame retardants exhibited a substantial and distinctive char residue.

Comparing the char residue between PP/14 %IFR/2 %LDH and PP/16 %LDHMPP, a notable distinction emerged. The char layer formed by PP/16 %LDHMPP exhibited fewer pores and greater density and

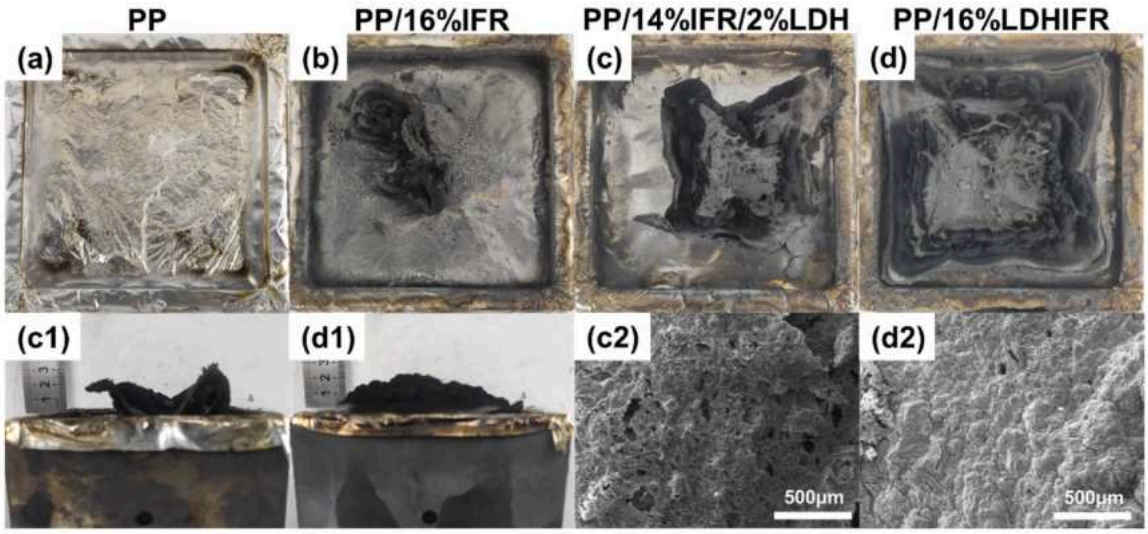


**Fig. 6.** Digital photos and SEM images of char residue after CCT tests: (a) PP, (b) PP/16 %IFR, (c, c1, c2) PP/14 %IFR/2 LDH and (d, d1, d2) PP/16 %LDHIFR.

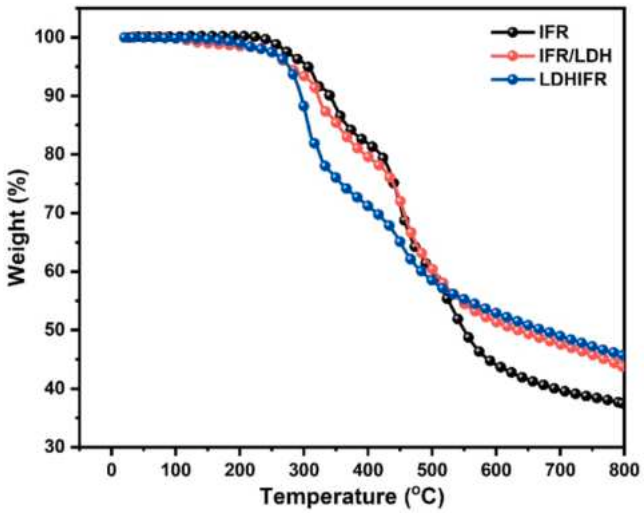


**Fig. 7.** TGA curves of IFR, IFR/LDH and LDHIFR under $N_2$ atmosphere.

**Table 6**
TGA data of flame retardants.

| Sample | $T_{5\ \%}$ (°C) | $T_{max}$ (°C) | Char yield at 700 °C (wt%) |
|---|---|---|---|
| IFR | 307 | 447 | 37.5 |
| IFR/LDH | 278 | 455 | 43.9 |
| LDHIFR | 278 | 303 | 46.2 |

integrity. SEM imaging vividly illustrated that the surface of the char layer formed by PP/14 %IFR/2 %LDH featured a more extensive pore structure. Conversely, the char layer of PP/16 %LDHMPP displayed a higher degree of completeness and density, effectively impeding the infiltration of external oxygen and heat into the underlying PP matrix. This resulted in a higher level of flame retardancy efficiency.

Fig. 7 presented the thermal decomposition results of different flame retardant formulations individually under $N_2$ atmosphere, with key data summarized in Table 6.

The initial decomposition temperature of IFR was 307 °C, significantly higher than that of IFR/LDH and LDHIFR, which followed the same pattern observed in PP composite materials. This indicated that the introduction of LDH promoted the early decomposition of the flame retardant.

Upon physically mixing Zn/Fe-LDH with IFR, the residue char content of the flame retardant increased. This enhancement was primarily attributed to the inherent inorganic properties of Zn/Fe-LDH, which catalyzed the self-charring of IFR.

Replacing MPP in IFR with Zn/Fe-LDH@MPP further increased the char yield to 46.2 %. This indicated that the co-precipitation of Zn/Fe-LDH on the surface of MPP was more conducive to synergistic flame retardancy, amplifying the catalytic charring effect, while simultaneously enhancing the dispersion of LDH in the PP.

The flame retardant system was further evaluated in an open environment. Fig. 8(a) and (b) presented digital images of the sample from different angles after combustion, while Fig. 8(c, d) and (e) displayed the SEM morphology of the char residue from IFR, IFR/LDH, and LDHIFR, respectively. Each of the flame retardant systems appeared the formation of an intumescent char layer following ignition. The char layer formed by pure IFR exhibited noticeable porosity. Upon the physical blending of Zn/Fe-LDH, the compactness of the IFR/LDH carbon layer improved, yet a porous structure was still observable. The char layer generated by LDHIFR showed a larger volume and a significant expansion effect. Additionally, SEM images of the char layer morphology revealed structures with greater density and integrity.

The superior self-charring effect of the composite material and flame retardant may be attributed to the fact that during combustion, some of the $Fe^{3+}$ and $Zn^{2+}$ in Zn/Fe-LDH@MPP reacted with the hydrocarbons in PP. Subsequently, at high temperatures, they undergo further oxidation–reduction to form amorphous metallic substances such as Fe, $Fe_3O_4$, and ZnO, respectively [41]. Some Fe combined with MPP to form $FePO_4$, which can fix more phosphorus elements during the residue formation process [42]. In a word, a more densely layered char structure effectively impeded the propagation of combustible materials and oxygen, ultimately enhancing the protection of the underlying substrate and slowing down the spread of fire.

### 3.5. *Mechanical properties*

The tensile test results for PP and its composites were illustrated in Fig. 9, while a comprehensive dataset, including impact strength values, was presented in Table 7. Upon the introduction of IFR into the PP matrix, the tensile strength decreased to 36.2 MPa, which was significantly lower than that of the original PP at 42.2 MPa. After the physical blending of Zn/Fe-LDH, due to the uneven aggregation of LDH, the elongation at break of the PP composite material continued to

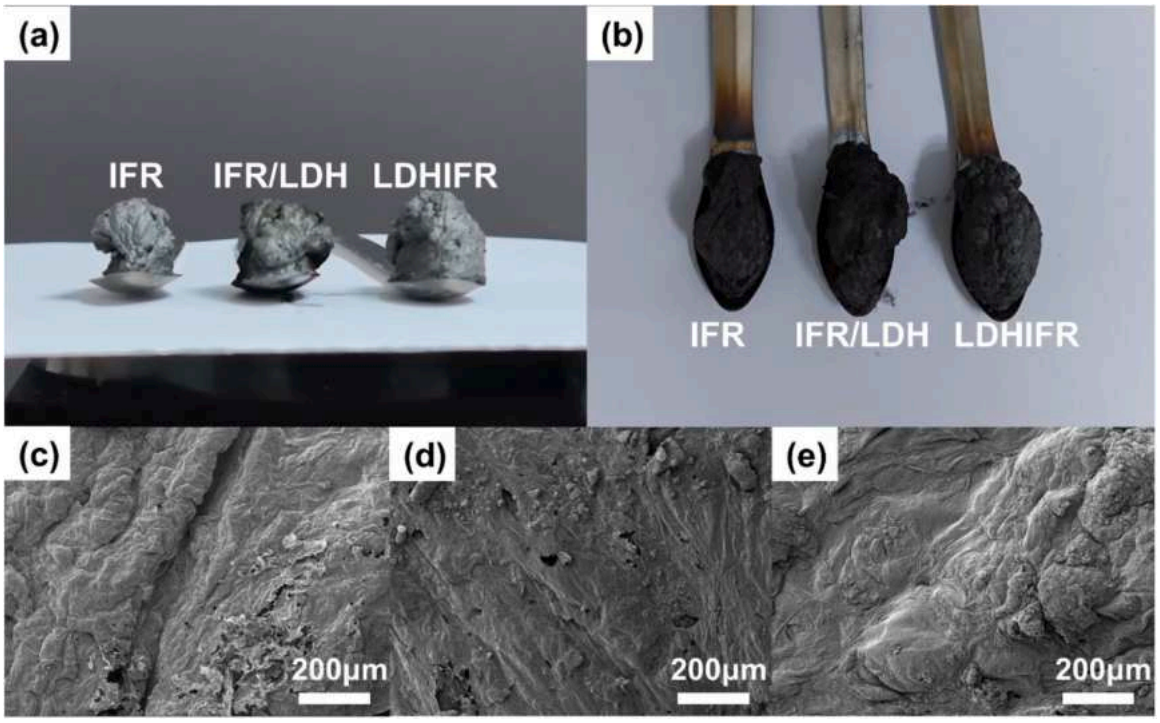


**Fig. 8.** (a) Front view, (b) top view and (c, d, e) SEM images of char residues from the open burning test.

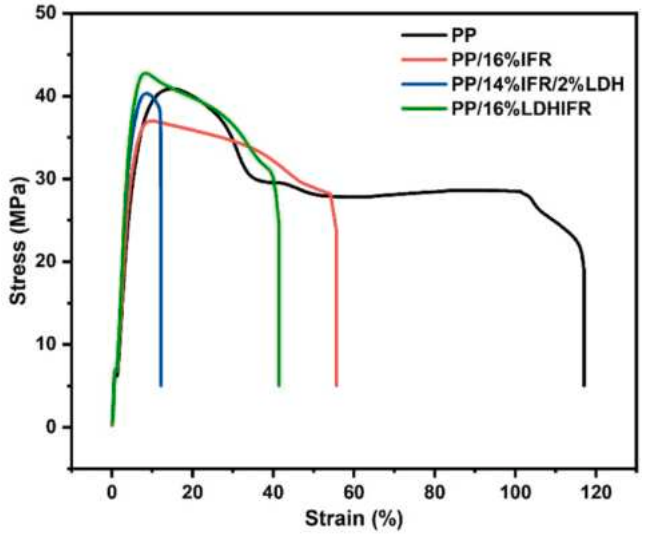


**Fig. 9.** Tensile test curves of PP and PP composites.

**Table 7**
Mechanical data for PP and PP composites.

| Sample | Tensile strength (MPa) | Elongation at break (%) | Impact strength (KJ/m$^2$) |
|---|---|---|---|
| PP | 42.2 ± 0.5 | 117.3 ± 0.8 | 3.7 ± 0.2 |
| PP/16 %IFR | 36.2 ± 0.4 | 55.8 ± 0.3 | 2.5 ± 0.1 |
| PP/14 %IFR/2 % LDH | 40.1 ± 0.6 | 12.2 ± 0.3 | 1.9 ± 0.2 |
| PP/16 %LDHIFR | 42.9 ± 0.3 | 41.6 ± 0.5 | 2.2 ± 0.1 |

significantly decrease, dropping to 12.2 %. In contrast, the tensile strength of PP/16 %LDHMPP reached 43.9 MPa, surpassing pure PP, with significantly improved elongation at break and impact strength compared to the samples containing IFR and IFR/LDH. This was attributed to the Zn/Fe-LDH@MPP exhibiting a rougher surface than MPP, providing a larger specific surface area and more interfacial interaction sites. This enhancement improved the interfacial interaction between MPP particles and the matrix, and eliminated the uneven mixing issue associated with direct blending of Zn/Fe-LDH.

As shown in Fig. 10(a), the binding between IFR and the matrix was not tight, resulting in IFR floating on the surface of the fracture, which significantly affected the mechanical properties of the material. Fig. 10 (b) illustrated the compatibility of Zn/Fe-LDH introduced at the interface with the matrix through physical blending. It can be clearly observed that Zn/Fe-LDH aggregated together, leaving a significant gap with the matrix, exhibiting a pronounced phase separation phenomenon. In PP/16 % LDHIFR, the surface of MPP in IFR was surrounded by Zn/Fe-LDH deposition, making the MPP surface rougher and increasing its specific surface area. This leads to a more uniform dispersion of rigid particles in the matrix, thereby improving the influence of introduced inorganic particles on the elongation at break and impact strength of the composite material.

## 4. Conclusion

This study synthesized a novel flame retardant, Zn/Fe-LDH@MPP, through an in-situ co-precipitation method and investigated its enhancement effect on the flame retardant and mechanical performances of PP when compounded with PAPP. The combination of PAPP and Zn/Fe-LDH@MPP demonstrated enhanced flame retardant performance in PP, with the LOI of PP/16 %LDHIFR composite reaching 32.7 %, achieving UL-94 V-0 rating. Furthermore, compared to pure PP, the pHRR, THR, and TSP of the PP/16 %LDHIFR were significantly reduced by 89.7 %, 41.4 %, and 37.7 %, respectively, while the char residue increased to 21.4 wt%. Meanwhile, the tensile strength of the samples could be maintained at 42.9 MPa, helping to mitigate the negative impact of flame retardant addition on the mechanical properties of the

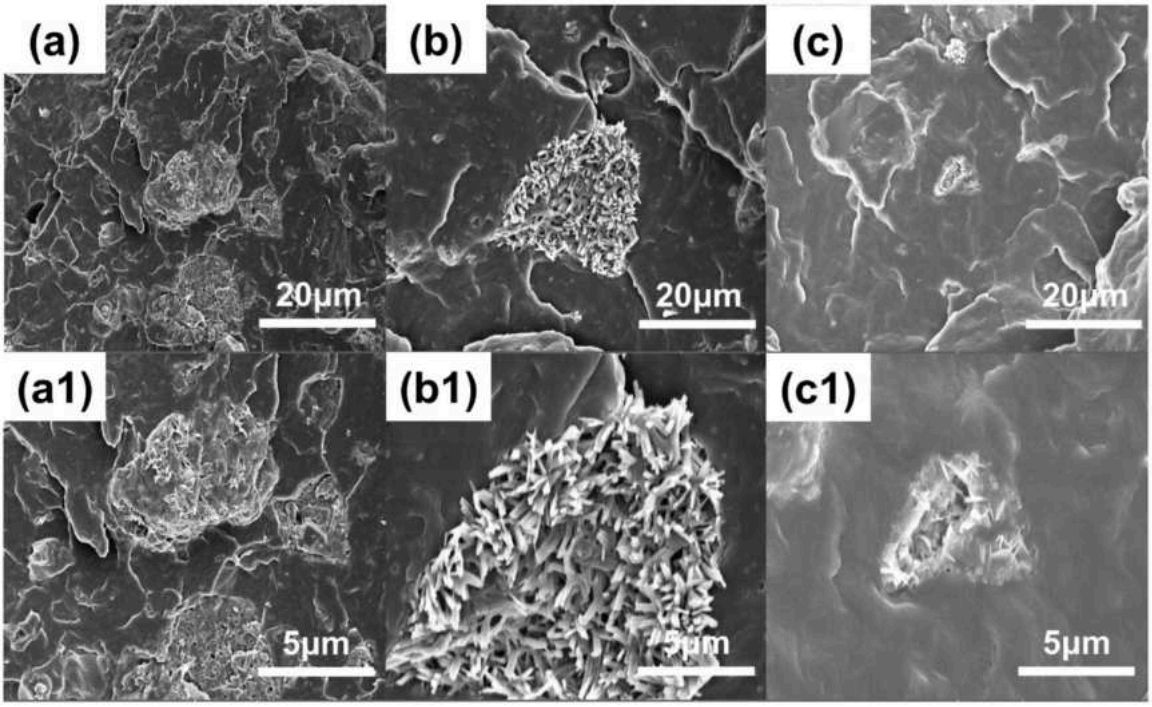


**Fig. 10.** The SEM images of (a) PP/16 %IFR, (b) PP/14 %IFR/2 % LDH and (c) PP/16 %LDHIFR elongated fracture surfaces.

composite material. With this simple modification method, PAPP/Zn/Fe-LDH@MPP was expected to become an effective alternative to traditional IFR.

## CRediT authorship contribution statement

**Zhishuo Liu:** Writing – original draft, Formal analysis, Data curation, Conceptualization. **Yifang Hua:** Resources, Methodology, Investigation, Data curation. **Suqin Liu:** Methodology, Investigation. **Hongfei Li:** Project administration, Methodology. **Xiaoyu Gu:** Supervision, Resources, Funding acquisition. **Jun Sun:** Writing – review & editing, Supervision, Resources, Funding acquisition. **Sheng Zhang:** Supervision, Resources, Conceptualization.

## Declaration of competing interest

The authors declare that they have no competing financial interests or personal relationships that appeared to influence the work reported in this paper.

## Acknowledgements

The authors would like to thank the financial support from the National Natural Science Foundation of China (Grant No. 52373051, and 22175017).

## Data availability

No data was used for the research described in the article.

## References

[1] S. Zhang, A.R. Horrocks, A review of flame retardant polypropylene fibres, Prog. Polym. Sci. 28 (11) (2003) 1517–1538.
[2] Z. Wang, K.G. Burra, T. Lei, A.K. Gupta, Co-pyrolysis of waste plastic and solid biomass for synergistic production of biofuels and chemicals-a review, Prog. Energy Combust. Sci. 84 (2021) 100899.
[3] O. Guselnikova, O. Semyonov, E. Sviridova, R. Gulyaev, A. Gorbunova, D. Kogolev, A. Trelin, Y. Yamauchi, R. Boukherroub, P. Postnikov, Functional upcycling" of polymer waste towards the design of new materials, Chem. Soc. Rev. 52 (14) (2023) 4755–4832.
[4] H. Huang, Z. Chen, J. Wang, P. Wei, Synergistic effects of sepiolite on intumescent flame retardant polypropylene, Express Polym. Lett. 4 (12) (2010) 743–752.
[5] Z. Fang, Z. Guo, H. Ma, Q. Chen, Y. Wu, Study of a halogen-free flame-retarded polypropylene composition with balanced strength and toughness, Int. J. Mater. Prod. Technol. 37 (2010).
[6] T.D. Huan, S. Boggs, G. Teyssedre, C. Laurent, M. Cakmak, S. Kumar, R. Ramprasad, Advanced polymeric dielectrics for high energy density applications, Prog. Mater. Sci. 83 (2016) 236–269.
[7] L. Lu, N. Guo, X. Qian, S. Yang, X. Wang, J. Jin, G. Shao, Thermal degradation and combustion behavior of intumescent flame-retardant polypropylene with novel phosphorus-based flame retardants, J. Appl. Polym. Sci. 135 (10) (2017) 45962.
[8] M. Deng, Z. Zhang, J. Sun, X. Liu, H. Li, X. Gu, S. Zhang, Improving the flame retardancy and water resistance of polypropylene by introducing microcapsule flame retardant system and modified zinc oxide, Polym. Degrad. Stab. 221 (2024) 110668.
[9] Y. Wang, R. Guo, J. Zhang, H. Wang, B. Niu, H. Yan, P/N/Si-rich and flexible coating imparting polypropylene excellent flame retardancy without compromising its inherent mechanical properties, Chem. Eng. J. 487 (2024) 150519.
[10] A.L. Margolin, T.V. Monakhova, P.M. Nedorezova, A.N. Klyamkina, S. V. Polschikov, Effects of graphene on thermal oxidation of isotactic polypropylene, Polym. Degrad. Stab. 156 (2018) 59–65.
[11] Y. Zhou, S. Qiu, L. Ding, F. Chu, W. Liu, W. Yang, W. Hu, Y. Hu, Innovative design of environmentally friendly silicon-based polyphosphazene-functionalized hydroxyapatite nanowires: an efficient enhancement strategy for the fire safety and mechanical properties of unsaturated polyester, Chem. Eng. J. 437 (2022) 135489.
[12] P. Song, Y. Shen, B. Du, M. Peng, L. Shen, Z. Fang, Interfaces, effects of reactive compatibilization on the morphological, thermal, mechanical, and rheological properties of intumescent flame-retardant polypropylene, ACS Appl. Mater. Interfaces 1 (2) (2009) 452–459.
[13] D. Tang, L. Zhu, X. Li, Y. Liu, Q. Wang, Improved flame resistance and thermal insulation properties of steel fireproof coatings based on polyvinyl alcohol @ expandable graphite, Prog. Org. Coat. 191 (2024) 108444.
[14] Y. Wang, C. Qu, K. Yu, Z. Si, J. Zhang, PTFE-based flame retardant coatings optimized by melamine polyphosphate/aluminum diethyl hypophosphite/anhydrous transparent powder through orthogonal experiment, Prog. Org. Coat. 191 (2024) 108423.
[15] F. Demiryuğuran, N. Usta, Synergistic effects of fly ash on thermal, combustion, and mechanical properties of polypropylene including intumescent flame retardant, J. Appl. Polym. Sci. 140 (48) (2023) e54716.
[16] J.F. Li, W. Jiang, Y. Gao, Synergistic P-N charring agents to enhance flame retardancy of ethylene-vinyl acetate (EVA): insights from experimental and molecular dynamic simulations, Polym. Degrad. Stab. 218 (2023) 110570.
[17] T. Chen, X. Xiao, J. Wang, N. Guo, Composites, fire, thermal and mechanical properties of TPE composites with systems containing piperazine pyrophosphate (PAPP), melamine phosphate (MPP) and titanium dioxide ($TiO_2$), Plast. Rubber Compos. 48 (12) (2019) 1–11.

[18] L. Li, Y. Huang, W. Tang, Y. Zhang, L. Qian, Synergistic effect between piperazine pyrophosphate and melamine polyphosphate in flame retardant coatings for structural steel, Polymers (Basel) 14 (18) (2022) 3722.
[19] Z. Yuan, H. Wen, Y. Liu, Q. Wang, Synergistic effect between piperazine pyrophosphate and melamine polyphosphate in flame retarded glass fiber reinforced polypropylene, Polym. Degrad. Stab. 184 (2021) 109477.
[20] Y. Sun, B. Yu, Y. Liu, F. Bai, J. Yan, J. Wang, F. Huang, S. Gao, Design of 2d charring-foaming agent for highly efficient intumescent flame retardant polylactic acid composites, Compos. Commun. 43 (2023) 101720.
[21] C. Zhu, M. He, Y. Liu, J. Cui, Q. Tai, L. Song, Y. Hu, Synthesis and application of a mono-component intumescent flame retardant for polypropylene, Polym. Degrad. Stab. 151 (2018) 144–151.
[22] W. Tang, L. Qian, Y. Chen, Y. Qiu, B. Xu, Intumescent flame retardant behavior of charring agents with different aggregation of piperazine/triazine groups in polypropylene, Polym. Degrad. Stab. 169 (2019) 108982.
[23] W. Zhang, W. Wu, H. Hu, J. Ye, Z. Wang, F. Xie, Synthesis of a highly efficient charring agent and its application to intumescent flame-retardant coatings for 3D-printed polypropyleneparts, J. Appl. Polym. Sci. 141 (23) (2024) e55456.
[24] X. Zhao, Y. Liu, B. Sun, Z. Liu, Z.B. Shao, X. Liu, H. Zhang, Z. Sun, W. Hu, Lignin-derived flame retardant for improving fire safety and mechanical properties of polypropylene, J. Appl. Polym. Sci. 140 (48) (2023) e54739.
[25] B. Hou, X. Song, K. Song, Z. Geng, Y.T. Pan, P. Song, R. Yang, Synchronous preparation and modification of LDH hollow polyhedra by polydopamine: Synthesis and application, J. Colloid Interface Sci. 654 (2024) 235–245.
[26] J. Ma, N. Yang, W. Li, Y. Zhou, X. Sun, Functional nanocomposite based on waterborne polyurethane and layered double hydroxide as a flame retardant for leather, J. Clean. Prod. 380 (2022) 134966.
[27] A.G. Sowndarya, S. Mandal, R. Prasanna, Phosphate intercalated Mg/Al layered double hydroxide nanosheets as a novel flame retardant for leather: synthesis, characterization, and application studies, Appl. Clay Sci. 230 (2022) 106714.
[28] X. Hong, Y. Zheng, Y. Shi, W. Zheng, F. Lin, L. Xiong, A facile strategy for constructing lightweight, fire safety and compression resistance poly(vinylalcohol) aerogels with highly-efficient expansible graphene oxide/layered double hydroxides hybrid synergistic flame retardant, J. Colloid Interface Sci. 650 (2023) 686–700.
[29] J. Hu, S. Xu, C.J. Ding, Z.H. Liu, W.J. Yan, Y. Hu, C.Z. Zhong, X.X. Cui, K. Wu, H. Y. Zeng, Novel carbon microspheres prepared by xylose decorated with layered double hydroxide as an effective eco-friendly flame retardant for polypropylene, Coll. Surf. A: Physicochem. Eng. Asp. 650 (2022) 129472.
[30] L. Wang, X.Y. Tian, Z.H. Liu, Q.Y. He, J.S. Li, S.C. Liu, J. Jian, S. Xu, Fabrication of highly hydrophobic layered double hydroxide decorated with tannic acid cross-linked phosphazene as a novel flame retardant for polypropylene, Coll. Surf. A: Physicochem. Eng. Asp. 667 (2023) 131356.
[31] S. Jiang, L. Liu, X. Yang, B. Li, M. Xu, Nickel-aluminum hydrotalcite for improving flame retardancy and smoke suppression of intumescent flame retardant polypropylene: preparation, synergy, and mechanism study, Macromol. Mater. Eng. 308 (4) (2022) 2200533.
[32] X. Jin, X. Gu, C. Chen, W. Tang, H. Li, X. Liu, S. Bourbigot, Z. Zhang, J. Sun, S. Zhang, The fire performance of polylactic acid containing a novel intumescent flame retardant and intercalated layered double hydroxides, J. Mater. Sci. 52 (20) (2017) 12235–12250.
[33] H. Ren, K. Qing, Y. Chen, Y. Lin, X. Duan, Smoke suppressant in flame retarded thermoplastic polyurethane composites: synergistic effect and mechanism study, Nano Res. 14 (11) (2021) 3926–3934.
[34] S. Huang, G. Wang, N. Li, H. Luo, Mechanism of the pH-induced aggregation reaction between melamine and phosphate, RSC Adv. 2 (29) (2012) 10948–10954.
[35] Y. Hua, J. Chen, J. Liu, J. Sun, X. Gu, S. Jiang, S. Zhang, Fabrication of a transparent, flame retardant, and antimicrobial epoxy resin by a novel phosphorus-containing Schiff base molecule, Polym. Degrad. Stab. 209 (2023) 110274.
[36] Y. Luo, S. Wang, X. Du, Z. Du, X. Cheng, H. Wang, Durable flame retardant and water repellent cotton fabric based on synergistic effect of ferrocene and DOPO, Cellulose 28 (3) (2021) 1809–1826.
[37] J. Xu, X. Li, X. Li, S. Li, L. Zhao, D. Wang, W. Xing, Z. Yan, Free-standing cotton-derived carbon microfiber@nickel-aluminum layered double hydroxides composite and its excellent capacitive performance, J. Alloys Compd. 787 (2019) 27–35.
[38] Z. Xu, G. Lu, Hydrothermal synthesis of layered double hydroxides (LDHs) from mixed MgO and $Al_2O_3$: LDH formation mechanism, Chem. Mater. 17 (5) (2005) 1055–1062.
[39] C. Chen, B. Wang, G. Xiao, F. Zhong, J. Zhou, M. Cao, Z. Yang, C. Chen, R. Zou, Flower-like Ni-Al/LDH synergistic polyaniline anchored to the carbon sphere surface to improve the fire performance of waterborne epoxy coatings, Prog. Org. Coat. 186 (2024) 108068.
[40] A. Zaher, M. Taha, A. Farghali, R. Mahmoud, Zn/Fe LDH as a clay-like adsorbent for the removal of oxytetracycline from water: combining experimental results and molecular simulations to understand the removal mechanism, Environ. Sci. Poll. Res. 27 (11) (2020) 12256–12269.
[41] Z.B. Shao, J. Cui, X.L. Li, J.L. Palencia, D.Y. Wang, Chemically inorganic modified ammonium polyphosphate as eco-friendly flame retardant and its high fire safety for epoxy resin, Compos. Commun. 28 (2021) 100959.
[42] W.X. Li, D.J. Liao, X.P. Hu, Z. Cheng, C.Q. Xie, Synergistic improvement of fire retardancy and mechanical properties of ferrocene-based polymer in intumescent polypropylene composite, Polym. Adv. Technol. 30 (9) (2019) 2402–2413.